machines

MDPI

Article

Analysis and Optimization of Flapping-Wing Mechanism Based on Genetic Algorithm

Yunyu Ling [1,2], Benyou Liu [3], Hongxin Zhang [1,2,*], Lan Bo [1,2] and Mingjie Liu [1,2]

[1] College of Mechanical and Electrical Engineering, Qingdao University, Qingdao 266071, China; lingyunyu@qdu.edu.cn (Y.L.); bolan@qdu.edu.cn (L.B.); liumingjie@qdu.edu.cn(M.L.)
[2] Power Integration and Energy Storage Systems Engineering Technology Center (Qingdao), Qingdao 266071, China
[3] Qingte Group Limited, Qingdao 266041, China; liubenyou@qingtegroup.com
* Correspondence: zhx@qdu.edu.cn

Abstract: Inspired by the wing-flapping action of birds, this study considers the inherent dynamics among vehicle mechanisms to optimize the vehicle's geometric parameters. The goal is for the vehicle to imitate the wing-flapping action of birds while minimizing energy consumption and the peak torque during flapping. To accomplish this, a dynamics model and an energy consumption model are established for the vehicle drive mechanism, followed by a multi-objective optimization under the boundary conditions of each parameter. Because of the complexity of the model, a mathematical tool that combines the genetic algorithm with the augmented Lagrange multiplier method is adopted in the optimization process. Simulation results show that the optimized energy consumption and peak moments are reduced. The proposed method provides a theoretical basis for designing a reliable flap-winged vehicle with reasonable parameter choices.

Keywords: flapping-wing vehicle; mechanical design; dynamics; lagrange multipliers; design optimization



Academic Editor: Carmine Maria Pappalardo

Received: 13 January 2025
Revised: 26 February 2025
Accepted: 26 February 2025
Published: 28 February 2025

Citation: Ling, Y.; Liu, B.; Zhang, H.; Bo, L.; Liu, M. Analysis and Optimization of Flapping-Wing Mechanism Based on Genetic Algorithm. *Machines* **2025**, *13*, 197. https://doi.org/10.3390/machines13030197

Copyright: © 2025 by the authors. Licensee MDPI, Basel, Switzerland. This article is an open access article distributed under the terms and conditions of the Creative Commons Attribution (CC BY) license (https://creativecommons.org/licenses/by/4.0/).

1. Introduction

Insects and birds have evolved to exhibit excellent flight capabilities and can fly efficiently in complex environments. Inspired by the flight of birds and insects, research on bionic vehicles has progressed rapidly in recent years [1]. Flapping-winged vehicles offer greater flexibility and adaptability than conventional fixed-wing and rotary-wing vehicles. They can perform tasks in tight or complex spaces and are often quieter and faster [2].

Flapping-wing vehicles are designed to generate thrust through the flapping and peeling of wings from one another, emulating the flapping motions of flying animals in nature. A significant number of bionic vehicles have been designed to mimic various species of flying creatures, including but not limited to butterflies [3], hummingbirds [4,5], and beetles [6]. The bionic flapping-wing crafts that have been designed differ in their imitation objects. The flapping mechanism of the flapping wing determines its movement. In its design process, based on the principle of bionics, the kinematics of the flapping mechanism all follow the morphology and kinematics of animals. The current bionic flapping-wing craft is based on the kinematics of the flapping wing developed in the form of the main soft actuators and artificial muscles [1,7,8], a string-driven [4,9,10] "linkage-slider" combination mechanism [5,11], a gear-driven linkage mechanism [12–15], a parallel crank-rocker mechanism [16], and the use of a single-degree-of-freedom crank-rocker mechanism to realize oscillation of the wings [17–20].

In the research and design of bionic vehicles, especially miniature flapping-wing micro air vehicles (FMAVs), it has been a constant pursuit of researchers to generate sufficient lift and large payloads with as little energy consumption as possible for the vehicle. Research spans from the study of the energy consumption mechanism of biological flight [21,22], such as the energy demand of insect flight [23], to the energy-saving design to reduce the energy consumption of flapping-wing vehicles [24–26]; however, the majority of the energy-saving designs to reduce the energy consumption of flapping-wing vehicles and thus increase their sustained flight time have focused on the design of an energy-saving and highly efficient airfoil [24–27]. When designing bionic aircraft structures, research has focused on imitating the object they are modelled after as much as possible [17–20], such as a bat-like flapping-wing vehicle with the dimensions and flapping-wing morphology of a bat [28]. After determining the drive mode of the bionic vehicle, the drive performance of the vehicle itself and its impact on the energy consumption of the flapping-wing vehicle are rarely considered. The drive structure is an important part of the flapping-wing vehicle, and a reliable structure can improve flight agility, reduce flight control coupling, improve flight efficiency, and even complete the flight mission [29]. For this reason, this paper is based on the selected bionic vehicle drive mode. Based on the selected bionic vehicle drive method, kinematic and dynamic analyses of its drive mechanism are carried out. The dynamics model of the vehicle drive mechanism to the wing is established, and on this basis, the energy consumption model and torque model of the vehicle drive mechanism are constructed. Finally, the energy consumption and the motor output torque are optimized for the structure of the drive mechanism of the bionic vehicle itself.

To enhance the flight performance of the flapping-wing vehicle and minimize energy consumption during flight and the wear and tear of the vehicle drive mechanism, this paper proposes an optimized design for the drive mechanism of the bionic vehicle. The contributions of this paper can be enumerated as follows: (1) the optimization design that considers the influence of the bionic vehicle drive mechanism on the flight performance of the flapping wing; (2) the establishment of a rigid-body dynamics model of the vehicle drive mechanism that is closer to the real kinematic characteristics of the drive mechanism; (3) the construction of a dynamics optimization model based on energy consumption and moments; and (4) the use of a combination of genetic algorithms and Lagrange multipliers to solve the optimization model.

The remainder is structured as follows. Section 2 provides a detailed exposition of the vehicle's structural and motion laws, an analysis of its kinematics and dynamics during oscillation, and the incorporation of an aerodynamic model of the simplified wing. The subsequent section is dedicated to formulating the basis for the ensuing optimization. Section 3 introduces the multi-objective optimization method, incorporating Lagrange multipliers to formulate the optimization objective through a weighting method. The subsequent section, Section 4, details the implementation of an iterative process to identify the optimal solution through the employment of a genetic algorithm. This approach is then validated through a comparison with the proposed optimization algorithm. Finally, Section 5 offers a comprehensive summary of the study's findings and discusses its limitations.

2. Modeling of Transmission System of Flapping-Wing Aircraft

In this section, the flapping-wing vehicle transmission mechanism is selected, followed by an analysis of the kinematics and dynamics of the transmission mechanism, which establishes the foundation for the subsequent optimization process.

2.1. Transmission System Structure

Among the common drive mechanisms for flapping-wing vehicles, soft-drive robotic actuators have been shown to have limited energy density and bandwidth, as well as greater difficulty in integration with rigid structures, which can cause a failure to lift off [7,8]. In addition, chord-based oscillating systems have been demonstrated to be more complex, inefficiently driven, and costly to manufacture [4,9,10]. In contrast, forms such as space link and link-slider combinations, as well as parallel mechanisms, have been shown to concentrate contact stresses, potentially leading to increased wear and tear, reduced efficiency, and even failure to take off [16]. The utilization of a single-degree-of-freedom crank-rocker mechanism to achieve oscillating wings offers a distinct advantage. This approach ensures simplicity and compactness in the structure while maintaining a low manufacturing cost and enabling hovering capabilities in flight [29]. Consequently, this paper proposes the utilization of the single-degree-of-freedom crank linkage mechanism as the transmission form for the flapping-wing vehicle.

As illustrated in Figure 1, two distinct sets of independent crank-rocker mechanisms are selected to function as the driving mechanism of the flapping-wing craft. The hollow cup motor drives the crank, and the output linkage (rocker) connects to the wing, thereby actuating the wings to flap and enabling the craft to fly.

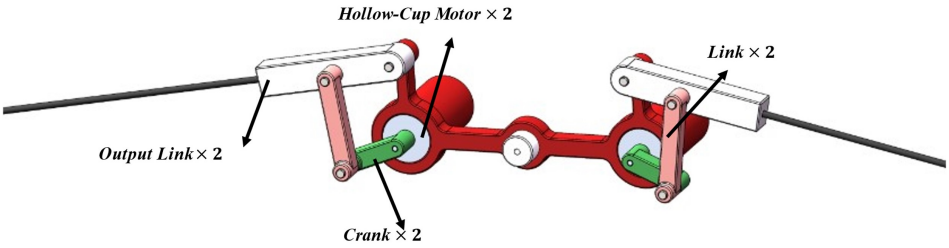


Figure 1. Flapping-wing aircraft crank-rocker drive mechanism.

2.2. Dynamic Process Modelling

To enhance the capacity of the flapping-wing flying vehicle to emulate the flight dynamics of animals, a comprehensive analysis of the kinematic mechanisms underlying its propulsion system is imperative. The position parameters and forces of the oscillating-wing drive mechanism are illustrated in Figure 2. In this figure, points A, B, C, and D represent the rotating joints. The connecting rod AD is the rack, which is fixed at joints A and D, and has a length of l_0. The connecting rod AB is the crank, with a length of l_1, driven by the hollow cup motor; it rotates about joint A, and its rotation angle is defined as θ_1. The rod BC is the connecting rod of the oscillating-wing drive mechanism, with a length of l_2, which rotates about joint B, and its rotation angle is θ_2. The rod DE is the rocker of the drive mechanism, with a length of l_3, which rotates about joint D. For the convenience of the following calculations, the rotation angle of DE is redefined as the rotation angle about joint C, and this angle is denoted by θ_3. The rod EF is the wing support rod, with a length of l_4, which is affixed to the drive mechanism (specifically, to the output rod DE). Finally, f represents the air resistance acting on the wing during flight.

The equation can be obtained by projecting the $ABCD$ closed vector equation in the plane x-y direction.

$$\begin{cases} l_1 \cos\theta_1 + l_2 \cos(\theta_2 - \pi + \theta_1) + l_3 \cos\theta_3/2 = l_0, \\ l_1 \sin\theta_1 + l_2 \sin(\theta_2 - \pi + \theta_1) + l_3 \sin\theta_3/2 = 0, \end{cases} \tag{1}$$

where l_3 represents the rocker. Its swing angle is

$$\theta_3 = (\alpha_1 + \alpha_2) - \frac{\pi}{2}. \tag{2}$$

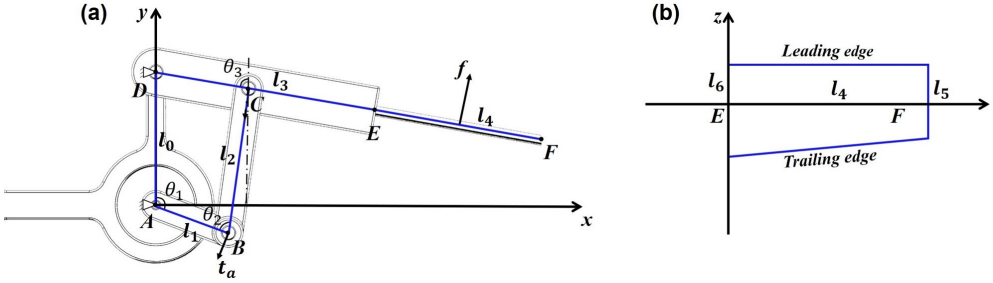


Figure 2. Coordinates of the flapping mechanism (**a**) and wing coordinates (**b**) of the wing-oscillating vehicle.

Angular velocity is

$$\dot{\theta}_3 = \left[\frac{a(a-\cos\theta_1)}{\alpha_3^2} + \frac{a\sin\theta_1}{\alpha_4^2}\left(2 - \frac{M^2}{\alpha_3^2}\right)\right]\dot{\theta}_1. \tag{3}$$

Angular acceleration is

$$\begin{aligned}\ddot{\theta}_3 = &\left[\frac{a(a-\cos\theta_1)}{\alpha_3^2} + \frac{a\sin\theta_1}{\alpha_4^2}\left(2 - \frac{M^2}{\alpha_3^2}\right)\right]\ddot{\theta}_1 \\ &+ \left\{\frac{a\sin\theta_1}{\alpha_3^2}\left[1 - \frac{2a(a-\cos\theta_1)}{\alpha_3^2}\right] + \frac{2a^2\sin^2\theta_1}{\alpha_4^2\alpha_3^2}\left(1 - \frac{M^2}{\alpha_3^2}\right)\right. \\ &\left. + 2\left(1 - \frac{M^2}{\alpha_3^2}\right)\frac{a\cos\theta_1 - 2a^2\sin^2\theta_1(2c^2 - M^2)}{\alpha_4^6}\right\}\dot{\theta}_1^2\end{aligned} \tag{4}$$

where

$$\begin{cases} \alpha_1 &= \tan^{-1}\left(\frac{a\sin\theta_1}{1-a\cos\theta_1}\right), \\ \alpha_2 &= \cos^{-1}\left(\frac{b^2-2a\cos\theta_1}{2\alpha_3 c}\right), \\ a &= \frac{l_1}{l_0}, \\ b &= \frac{l_0^2+l_1^2+l_3^2-l_2^2}{l_0^2}, \\ c &= \frac{l_3}{l_0}, \\ \alpha_3^2 &= 1 + 2a^2\cos\theta_1, \\ M &= b^2 - 2a\cos\theta_1, \\ \alpha_4^2 &= \sqrt{4\alpha_3^2 c^2 - M^2}. \end{cases} \tag{5}$$

where θ_1 is the rotation angle of the crank. In this paper, the bionic vehicle flies at a constant speed, the crank rotates at a constant speed, and the rotation frequency is 1.67 Hz. The time derivative of the projection Equation (1) yields the angular velocity $\dot{\theta}_2$ of the connecting rod l_2 and the angular acceleration $\ddot{\theta}_2$.

The crank is supposed to rotate at an angle θ_1 as the generalized variable Θ, and the dynamics of the linkage mechanism are analyzed using Lagrange's equation to obtain the generalized driving torque τ:

$$\tau = \frac{d}{dt}\left(\frac{\partial L}{\partial \dot{\Theta}}\right) - \frac{\partial L}{\partial \Theta}, \tag{6}$$

where

$$L(\Theta, \dot{\Theta}) = K(\Theta, \dot{\Theta}) - U(\Theta),$$

$L(\Theta, \dot{\Theta})$ is the Lagrangian, $K(\Theta, \dot{\Theta})$ is the kinetic energy of the system, and $U(\Theta)$ is the potential energy of the system.

I_1 is the moment of inertia of the link where the crank is located, $\dot{\theta}_1$ is its rotational angular velocity vector, and m_i is the mass of each linkage (with m_3 being the equivalent mass of the rocker arm and the wing). I_i is the inertia tensor of each linkage and P_i is the center of mass position vector of each linkage. The center of mass velocity vector v_i is obtained by differentiating P_i with respect to time, and θ_i is the angular velocity of each linkage and the wing. Assuming that the material of the drive mechanism is homogeneous, the kinetic energy of the system is

$$K = \frac{1}{2}\sum_{i=1}^{n}\left(m_i v_i^T v_i + \dot{\theta}_i^T I_i \dot{\theta}_i\right). \tag{7}$$

Taking g as the gravity vector and U_{ref_i} as a constant related to the choice of the zero potential energy point, and selecting the plane depicted in Figure 2a (which coincides with the x-axis and is perpendicular to the y-axis) as the zero potential energy surface, the total potential energy of the system is

$$U = \sum_{i=1}^{n}\left(-m_i g P_i + U_{\mathrm{ref}_i}\right). \tag{8}$$

The wing shape is shown in Figure 2b. The wing support bar l_4 is attached to the leading edge of the wing and has a length of 11 cm. It is important to note that the leading edge of the wing is not parallel to the trailing edge of the wing. The right side of the wing (l_5) is measured at 4.5 cm, while the chord length (l_6) is 7 cm. The wing area (S) can be calculated from the dimensions of the wing, and the linear speed v of the wing motion is

$$v = \left[\frac{l_4\,(2l_5 + l_6)}{3(l_5 + l_6)} + l_3\right]\dot{\theta}_3. \tag{9}$$

Let each link be a two-force rod, ρ the density of the air, and C_w the coefficient of drag, the value of which was derived from previous experiments [30], and the value of this coefficient was shown to be applicable for Reynolds numbers of the order of 10^4 [31]. The air resistance at low speed is

$$f = \frac{\rho\, C_w\, S\, v^2}{2}.$$

The direction of the air resistance f is perpendicular to EF, acting on the geometric center of the wing. Its direction is perpendicular to the plane of the wing and opposite to the movement direction of the wing, and its point of application is located on the extension line of the link DE. In this paper, the assumption of a uniform drag distribution is used, which implies that the geometric center coincides with the point of drag application. The unsteady effects of the vortex structure are not discussed in this paper due to the simplification of our model.

The wing is mounted with its geometric center positioned on the extension of the linkage DE. It is hypothesized that the fuselage of the bionic flapping-wing craft is parallel to the x-axis. As illustrated in Figure 2a, the air resistance is denoted by f, its direction is perpendicular to EF, and its point of action is situated on the extension line of the connecting

rod DE. Assuming that the motor force is t_a, with the point of action at the rotating joint B, and that its direction is perpendicular to the connecting rod AB, and considering that the connecting rods are two-force rods, the torque generated by the motor force t_a and that generated by the air resistance f are balanced with each other at the rotating joint D:

$$f\left[\frac{l_4\,(2l_5+l_6)}{3(l_5+l_6)}+l_3\right]=\frac{l_3}{2}\,t_a\,|\sin(\theta_1-\theta_2)\cos\phi|. \tag{10}$$

Accordingly, the external torque required to overcome air resistance can be calculated using the following equation:

$$T_m=t_a\,l_1=\frac{f\,l_1\left[\frac{l_4\,(2l_5+l_6)}{3(l_5+l_6)}+l_3\right]}{\frac{l_3}{2}|\sin(\theta_1-\theta_2)\cos\phi|}. \tag{11}$$

where

$$\phi=\frac{\pi}{2}-\cos^{-1}\left(\frac{l_2^2+l_3^2-l_{BD}^2}{2l_2l_3}\right). \tag{12}$$

The joint torque can be obtained from Equations (6)–(9):

$$\begin{aligned}\tau&=M(\Theta)\ddot{\Theta}+V(\Theta,\dot{\Theta})+G(\Theta)+T_m \\ &=\begin{bmatrix}M_1,M_2,M_3\end{bmatrix}\begin{bmatrix}\ddot{\Theta}_1\\ \ddot{\Theta}_2\\ \ddot{\Theta}_3\end{bmatrix}+\begin{bmatrix}V_1,V_2,V_3\end{bmatrix}\begin{bmatrix}\dot{\Theta}_1\\ \dot{\Theta}_2\\ \dot{\Theta}_3\end{bmatrix}+\begin{bmatrix}V_4,V_5,V_6\end{bmatrix}\begin{bmatrix}\dot{\Theta}_1\dot{\Theta}_1\\ \dot{\Theta}_1\dot{\Theta}_2\\ \dot{\Theta}_1\dot{\Theta}_3\end{bmatrix}+G+T_m\end{aligned} \tag{13}$$

where

$$\begin{cases}M_1 &= \left(\frac{m_1}{2}+m_2+m_3+m_4\right)l_1^2,\\ M_2 &= \left(\frac{m_2}{2}+m_3+m_4\right)l_1l_2\cos(\theta_1-\theta_2),\\ M_3 &= \frac{m_3+m_4}{2}\,l_1l_3\cos(\theta_1-\theta_3),\\ V_1 &= 0,\\ V_2 &= -\left(\frac{m_2}{2}+m_3+m_4\right)l_1l_2\left(\dot{\theta}_1-\dot{\theta}_2\right)\sin(\theta_1-\theta_2),\\ V_3 &= -\frac{m_3+m_4}{2}\,l_1l_3\left(\dot{\theta}_1-\dot{\theta}_3\right)\sin(\theta_1-\theta_3),\\ V_4 &= 0,\\ V_5 &= \left(\frac{m_2}{2}+m_3+m_4\right)l_1l_2\sin(\theta_1-\theta_2),\\ V_6 &= \frac{m_3+m_4}{2}\,l_1l_3\sin(\theta_1-\theta_3),\\ G &= -\left(\frac{m_1}{2}+m_2+m_3+m_4\right)g\,l_1\cos\theta_1.\end{cases} \tag{14}$$

Here, $M(\Theta)$ is the mass matrix, $V(\Theta,\dot{\Theta})$ is the centrifugal and Coriolis force vector, $G(\Theta)$ is the gravity vector, and T_m is the external torque.

The energy consumed by a flapping-wing aircraft during a single flapping period, designated as T, can be calculated as follows:

$$E=\frac{1}{\eta}\int_0^T\tau\,\dot{\theta}_1\,dt, \tag{15}$$

where η is the energy conversion factor of the hollow cup motor and takes the value of 0.78.

3. Structural Design Optimization Modelling

In this section, the dynamics optimization model of the transmission mechanism of a flapping-wing vehicle is established, and the optimization model is unconstrained. And a new multi-objective optimization method is proposed.

3.1. Design Variables

Since the dimensional parameters of the motor in the assembly position of the vehicle and the locations of joints A and D have been fixed, the size of the connecting rod l_0 (where AD is located) is fixed. Thus, the design variables of the dimensional parameters of the vehicle transmission mechanism are $X = [l_1, l_2, l_3]$.

3.2. Objective Function

3.2.1. Minimum Motor Output Torque

It can be seen that there is a positive correlation between the output torque of the selected motor and the flight performance of the vehicle. Furthermore, a reduction in the mass of the selected motor type will lead to an improvement in the flight performance, load-carrying capacity, and range of the flapping-wing vehicle. This is due to the fact that the air resistance exerted on the wing is reduced, assuming that all other conditions remain equal. Consequently, the peak crank linkage mechanism input torque [32] is identified as a key optimization objective.

$$N_1(x) = \min\ \tau_{\max} \tag{16}$$

3.2.2. Minimum Energy Consumption in Flight

In the course of flight, the flapping-wing aircraft must overcome air resistance and the energy expenditure associated with its own weight and gravity. The primary source of energy for this is the drive mechanism, which is responsible for propelling the aircraft through its movements. Consequently, reducing the energy consumption of the drive mechanism during flight can enhance the endurance of the aircraft. To this end, the objective function of the motor energy consumption of the vehicle drive mechanism in a flapping period has been established.

$$N_2(x) = \min\ E \tag{17}$$

3.3. Constraint

3.3.1. Rod Length Constraint

The constraints on rod length are determined by reference to the ratio of the structural dimensions of the bird's wings to the dimensions of the transmission gears where the cranks are located. These constraints are implemented by ensuring that the parameters of the rod dimensions of the transmission mechanism fall within the range specified by the conventional design of the vehicle and its final performance. Additionally, the constraints allow for the estimation of the range within which optimal values may occur.

$$\begin{cases} 10\,\text{mm} \le l_1 \le 30\,\text{mm}, \\ 10\,\text{mm} \le l_2 \le 50\,\text{mm}, \\ 10\,\text{mm} \le l_3 \le 50\,\text{mm}. \end{cases} \tag{18}$$

3.3.2. Conditions for the Existence of the Crank

In accordance with the operational parameters of the crank-rocker mechanism, the aggregate length of the shortest and longest rods in a four-link mechanism must be less than the sum of the remaining two rods.

$$\begin{cases} l_1 - l_0 \leq 0, \\ l_1 - l_2 \leq 0, \\ l_1 - l_3 \leq 0, \\ l_1 + l_0 - l_2 - l_3 \leq 0, \\ l_1 + l_2 - l_3 - l_0 \leq 0, \\ l_1 + l_3 - l_2 - l_0 \leq 0. \end{cases} \tag{19}$$

3.3.3. Oscillating Angle Amplitude

The angle at which different flying creatures flap their wings during flight varies; however, the majority flap their wings between 40° and 70°. To more accurately replicate the flight mechanics of these creatures, the flapping angle of the output bar DE must fall within this range [12].

$$\Delta\theta_3 \in (40^\circ, 70^\circ) \tag{20}$$

3.3.4. The Ratio of Air Return Stroke to Working Stroke

Most flying organisms require more time for the wing-down process than the wing-up process during a wing-flapping cycle. The drive mechanism of the bionic flapping-wing aircraft converts the circular motion of the drive motor into the flapping of the wing, and the time consumed in the working stroke during the motion should also be greater than the time consumed in the empty return stroke. The ratio of air return stroke to working stroke is given by

$$K = \frac{\pi + \theta}{\pi - \theta} \in (1.05, 1.25), \tag{21}$$

where

$$\theta = \cos^{-1}\left(\frac{(l_2 - l_1)^2 + l_0^2 - l_3^2}{2l_0(l_2 - l_1)}\right) - \cos^{-1}\left(\frac{(l_1 + l_2)^2 + l_0^2 - l_3^2}{2l_0(l_1 + l_2)}\right). \tag{22}$$

3.3.5. Transmission Angle Constraints

In order to guarantee optimal transmission efficiency for the four-link mechanism during its operational movement, it is essential to ensure that the transmission angle (μ) and the pressure angle are within an appropriate range [32]:

$$\mu \in (40^\circ, 140^\circ), \tag{23}$$

where

$$\mu = \cos\left(\frac{l_0^2 + l_1^2 - l_2^2 - l_3^2 - 2l_0l_1\cos\theta_1}{-2l_2l_3}\right). \tag{24}$$

3.4. Multi-Objective Optimization Model

Since the angular velocity term $\dot{\theta}$ and angular acceleration term $\ddot{\theta}$ need to be solved in the optimization model, there are two different velocity terms $\dot{\theta}_i$ ($i = 2, 3$) and angular acceleration terms $\ddot{\theta}_i$ ($i = 2, 3$) for the same crank position θ_1 for one wing-flapping cycle of the bionic flapping-wing vehicle. Both of these solutions are appropriate for the flapping-wing vehicle mechanism. However, these solutions are arranged and combined in the optimization code written, which does not follow the laws of motion of the mechanism. Moreover, due to the existence of singular points [33,34], the optimized target moment will appear to increase abruptly to infinity at the singular points. This causes the genetic algorithm to be difficult to converge, so in this paper the non-linear multi-constraint problem is trans-

formed into an unconstrained problem by a Lagrange multiplier method [35,36], and the optimal size of the four-bar mechanism is obtained by using the genetic algorithm [37]. The following is the mathematical model:

$$\begin{cases} \min\ z(x), \quad x \in \mathbb{R}^n, \\ \text{s.t.} \quad g_i(x) \le 0, \quad i = 1, 2, \ldots, m. \end{cases} \tag{25}$$

The introduction of slack variables $q = [q_1, q_2, \ldots, q_m]^T$ transforms the inequality-constrained problem into an equality-constrained problem.

$$\begin{cases} \min\ z(x), \quad x \in \mathbb{R}^n, \\ \text{s.t.} \quad g_i(x, q) = 0, \quad i = 1, 2, \ldots, m. \end{cases} \tag{26}$$

Subsequently, the equality-constrained Lagrange multiplier function of Equation (26) is constructed, and it takes the following form:

$$\begin{aligned} Z(x, y, \lambda, r) &= z(x) + \sum_{i=1}^{m} \lambda_i g_i'(x, q) + \frac{r}{2} \sum_{i=1}^{m} \left[g_i'(x, q) \right]^2 \\ &= z(x) + \sum_{i=1}^{m} \lambda_i \left[g_i(x) + q_i^2 \right] + \frac{r}{2} \sum_{i=1}^{m} \left[g_i(x) + q_i^2 \right]^2 \end{aligned} \tag{27}$$

For the function $Z(x, y, \lambda, r)$ to take an extreme value with respect to q, let $\nabla_q Z(x, y, \lambda, r) = 0$; then, the solution of the slack variable can be obtained. According to the solution, the slack variable can be obtained as

$$g_i(x) + q_i^2 = \begin{cases} g_i(x), & \text{if } g_i(x) \ge -\lambda_i / r, \\ -\lambda_i / r, & \text{if } g_i(x) < -\lambda_i / r. \end{cases} \tag{28}$$

The integration of the two cases of Equation (28) into the summation part of Equation (29) results in

$$Z(x, y, \lambda, r) = z(x) + \sum_{i=1}^{m} \lambda_i \eta_i + \frac{r}{2} \sum_{i=1}^{m} \lambda_i \eta_i^2, \tag{29}$$

where

$$\begin{cases} \eta_i = \max\left(g_i(x), -\frac{\lambda_i}{r} \right), \\ \lambda_i^{k+1} = \lambda_i^k + r\, \eta_i^k. \end{cases} \tag{30}$$

Here, λ_i represents the Lagrange multiplier, and the penalty factor, denoted as r, is a parameter that can be adjusted according to the specific circumstances of the problem at hand. The magnitude of the solution space is contingent upon the nature of the problem and the number and severity of constraints. If the penalty factor is set to a value that is too small, it may result in the algorithm converging at a slower rate or failing to reach the optimal solution. If the penalty factor is set to an excessive value, it may result in instability or the generation of numerical errors in the algorithmic process. Following a series of trials, the value of the penalty factor r is incrementally modified with the objective of ensuring the convergence of the optimization algorithm and the alteration of the objective function value.

$$r = (r^*). \tag{31}$$

3.5. Optimization Results Synthesis

In light of the aforementioned constraints and objective functions, two optimization models of the flapping-wing vehicle's transmission mechanism have been formulated, each tailored to a specific optimization objective.

$$\begin{cases} \min\ N_1(x), \\ X_1 = (l_1, l_2, l_3). \end{cases} \tag{32}$$

$$\begin{cases} \min\ N_2(x), \\ X_2 = (l_1, l_2, l_3). \end{cases} \tag{33}$$

The final optimization result is obtained by summing the aforementioned two sets of parameters with varying weights:

$$X = \omega_1 X_1 + \omega_2 X_2, \tag{34}$$

where ω_1 and ω_2 are the weighting factors. The initial value of the weighting factors is taken as 0.5. After analyzing the results of multiple iterations, the optimized weighting factors are determined to be $\omega_1 = 0.5$ and $\omega_2 = 0.5$.

4. Results Evaluation

The optimization objective is a complex non-linear function with process variables in the constraint function, which presents a significant challenge for conventional optimization algorithms. Consequently, a genetic algorithm [37] is employed to address this issue. This is a genetic algorithm designed for complex search spaces and non-linear optimization problems. The quality of the individuals (candidates for the solution) is enhanced continuously through generation-by-generation evolution, utilizing the operations of selection, crossover, and mutation. This enables the identification of the optimal solution or a set of optimal solutions. This advantage is particularly evident when confronted with a multitude of real-world problems.

The optimization process is shown in Figure 3, where the angle θ, angular velocity $\dot{\theta}$, and angular acceleration $\ddot{\theta}$ of each rod are obtained from the rigid body kinematics model of the flapping mechanism of the bionic vehicle. Then, the drive torque τ is obtained from the multi-rigid body kinematics model of the flapping mechanism and the aerodynamic model of the wing. However, there are multiple solutions when solving for the values of angular velocity $\dot{\theta}$ and angular acceleration $\ddot{\theta}$ in the MATLAB program. These solutions are iterative and do not conform to the laws of motion of the mechanical structure. In the case of a wing-oscillating vehicle, when the drive mechanism moves to singular points, the moment changes to infinity. At this point, the moments obtained appear as shown in Figure 4a. These solutions are defined as invalid solutions in Figure 3 and must be removed with additional checks. After removing the invalid solutions and limiting the torque values at the singular point, the results are shown in Figure 4b. In the iterative process as shown in Figure 3, $|\nabla_{x_j} Z^k(x, \lambda, r)|$ is the gradient function of the optimization objective. δ is the iteration factor, which refers to the best population in each generation of the genetic algorithm. δ tends to be infinitesimal as the number of iterations increases.

A set of flapping-wing vehicle transmission mechanism dimensions were derived through the simulation of the wingtip flight and oscillating characteristics of the flapping-wing vehicle. The size parameters are $l_1 = 12\,\text{mm}$, $l_2 = 31\,\text{mm}$, $l_3 = 30\,\text{mm}$, and $l_4 = 38\,\text{mm}$. The vehicle is designed to have a transmission mechanism, a tail mechanism, idler wheel pairs in the transmission mechanism, and gears where the cranks are

located. The latter are of the modulus of 0.5 and are plastic gears used for the power transmission. The primary control unit is an STM32F407, while the attitude sensor is an MPU06050, which is linked to the aforementioned control unit via the IIC bus. As illustrated in Figure 5, the controller employs the ERLS module for 2.4 GHz wireless communication with the host computer and remote control. The vehicle drive mechanism is powered by an 816 hollow cup motor, with the driver chip utilizing the TB6612. The tail is driven by an AFRC-D1602 micro servo. At the software level, FreeRTOS scheduling for the STM32 is employed for the purpose of multitasking.

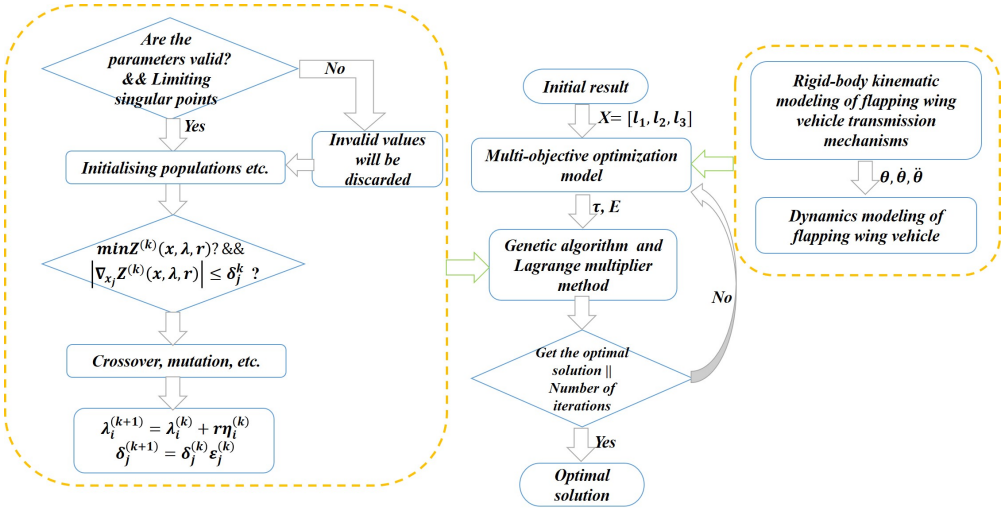


Figure 3. Optimization process overview.

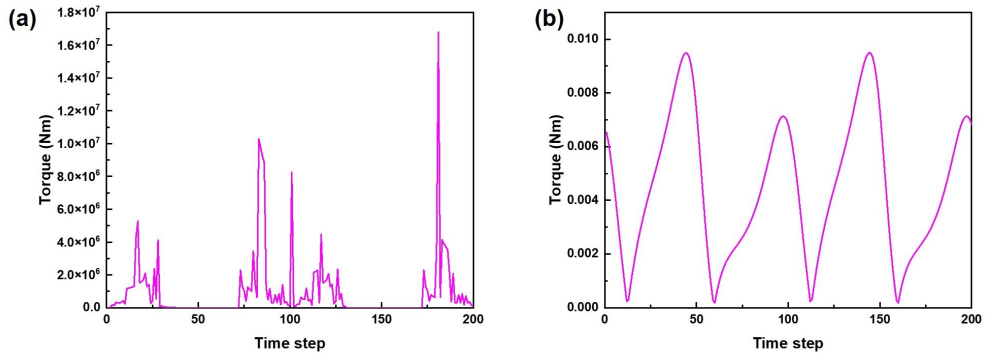


Figure 4. Torque, (**a**) with data at singular points, and (**b**) with selected positions.

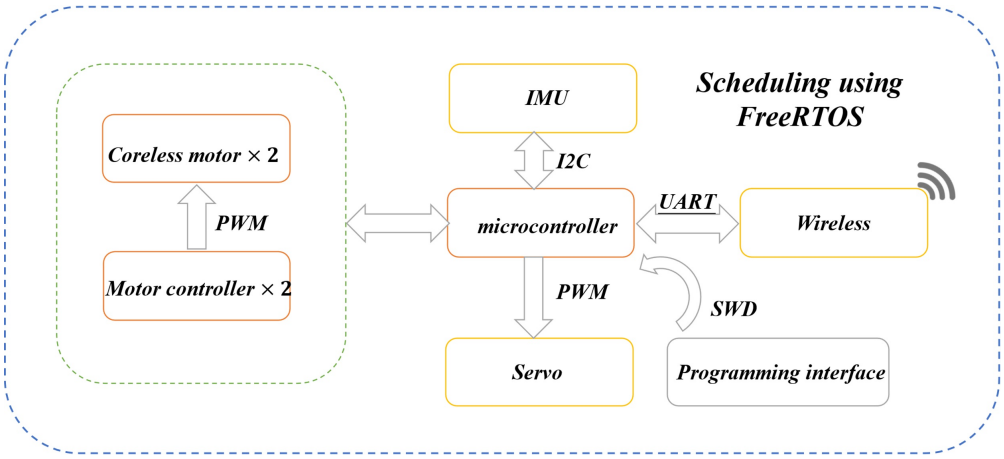


Figure 5. Electronics overview.

The original design size parameters were used as the initial parameters of the optimization process to generate the initial population, which consisted of 100 individuals. The number of iterations was set to 200, with a crossover probability of 0.8 and a mutation probability of 0.1. The resulting optimization is illustrated in Figure 6a; after 40 iterations, $N_1(x)$ converges and stabilizes at approximately 33.85, yielding final results of $l_1 = 0.010699$ m, $l_2 = 0.02522$ m, and $l_3 = 0.03489$ m. After rounding, these values become $l_1 = 11$ mm, $l_2 = 25$ mm, and $l_3 = 35$ mm. Similarly, as illustrated in Figure 6b, $N_2(x)$ converges after 55 iterations, with the corresponding value stabilizing at approximately 326.7; the final results in this case are $l_1 = 0.01223$ m, $l_2 = 0.03622$ m, and $l_3 = 0.03480$ m, which round to $l_1 = 12$ mm, $l_2 = 36$ mm, and $l_3 = 35$ mm. The comprehensive optimization results for the two groups of dimensions are presented in Table 1, and the final optimized size is calculated by summing the weights of each dimension, resulting in $l_1 = 11$ mm, $l_2 = 31$ mm, and $l_3 = 35$ mm.

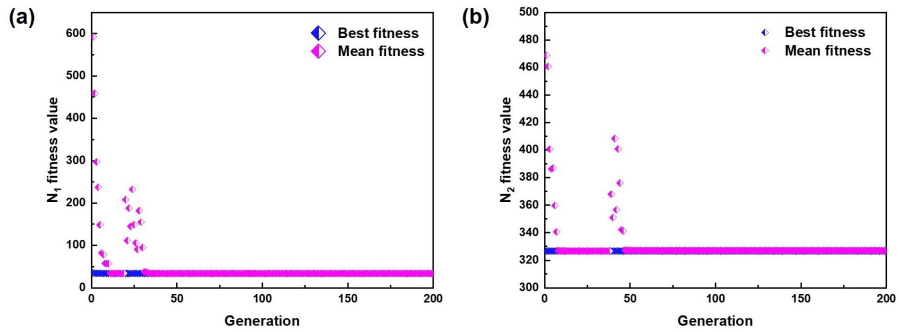


Figure 6. Genetic algorithm optimization process diagram.

Table 1. Comparison of flapping-wing vehicle dimensions.

Parameter	Original Result	Optimal Result
l_1	12 mm	11 mm
l_2	31 mm	31 mm
l_3	30 mm	35 mm

The results of the optimization process, along with the initial outcomes in terms of torque and power consumption in a single flapping cycle, are presented in Figure 7. It can be observed that the optimized dimensions result in a reduction in the peak torque compared to the original configuration, and the torque throughout a single cycle becomes more consistent. Table 2 illustrates that the optimized transmission mechanism exhibits a decreased peak motor drive torque, reducing from 0.00849 N·m to 0.00480 N·m, which represents a 43.49% reduction. Additionally, the motor energy consumption in a single flapping stroke declines from 9.20214 W to 4.85506 W, corresponding to a 47.24% decrease.

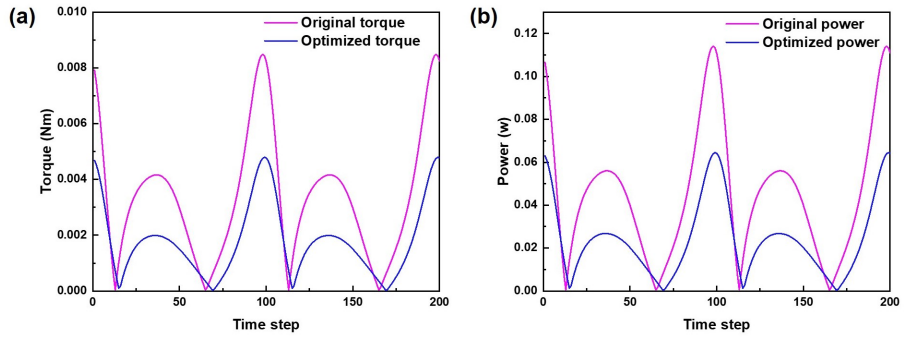


Figure 7. Motor torque, (**a**) and power consumption, (**b**) in a single flapping cycle.

Table 2. Comparison of flapping-wing vehicle performance.

Parameter	Original Result	Optimal Result
Driving peak torque	0.00849 N·m	0.00480 N·m
Total energy consumption for a tapping cycle	9.20214 w	4.85506 w

5. Conclusions

In order to enhance the flight capability of the flapping-wing vehicle, the genetic algorithm is employed to optimize the energy consumption and peak torque during the wing-flapping process. Prior to the optimization process, a comprehensive analysis was conducted on the flapping structure and motion law of the bionic vehicle. This was followed by the development of a more sophisticated computational model of the flapping mechanism dynamics, while a simplified wing aerodynamic model was introduced. Further improvements were made to the flapping-wing dynamics model. Furthermore, based on the aforementioned dynamics model, optimization problems pertaining to flight energy consumption and peak torque were established, taking into account the constraints imposed by each parameter. The genetic algorithm was enhanced through the incorporation of the Lagrangian method to address the presence of singular points. The results demonstrate that the optimized peak torque can be reduced from 0.00849 N·m to 0.00480 N·m, and the energy consumption can be reduced from 9.20214 W to 4.85506 W, indicating that the optimized parameters can achieve smoother moments and reduced energy consumption. The research presented in this paper addresses the flight dynamics of the flapping-wing vehicle, offers a theoretical foundation for the optimal design of the bionic vehicle's structure, and is conducive to enhancing the flight performance of the bionic vehicle.

Author Contributions: Conceptualization, Y.L. and H.Z.; methodology, Y.L.; software, Y.L.; validation, Y.L., B.L. and L.B.; formal analysis, M.L.; investigation, L.B.; resources, H.Z.; data curation, M.L.; writing—original draft preparation, Y.L.; writing—review and editing, Y.L.; visualization, L.B.; supervision, M.L.; project administration, H.Z.; funding acquisition, H.Z. All authors have read and agreed to the published version of the manuscript.

Funding: This research received no external funding.

Data Availability Statement: The datasets generated during and/or analyzed during the current study are not publicly available due to their containing information that could compromise the privacy of research participants but are available from the corresponding author on reasonable request.

Conflicts of Interest: Though some of the co-authors are employees of companies. The paper reflects the view of the scientists and not the company.

Nomenclature

The following abbreviations and symbols are used in this manuscript:

l_1, l_2, l_3, l_4	Length of the flapping-wing vehicle frame, the crank, the connecting rod, the rocking rod, and the wing
$\theta_1, \theta_2, \theta_3, \theta_4$	Angle of each rod with respect to the coordinate system of the frame
f	Air resistance experienced by the wing during the flight
τ	Generalized driving torque
I_1, I_2, I_3, I_4	Inertia tensor of each linkage
P_1, P_2, P_3, P_4	Center of mass position vector of each linkage
$L(\Theta, \dot{\Theta})$	Lagrangian quantity

$K(\Theta, \dot{\Theta})$	Kinetic energy of the system
$U(\Theta)$	Potential energy of the system
g	Gravity
U_{refi}	Constant related to the choice of the zero potential energy point
C_w	Drag coefficient
S	Wing area
v	Linear speed of wing
$M(\Theta)$	The mass matrix
$C(\Theta, \dot{\Theta})$	Centrifugal and Coriolis force vector
$G(\Theta)$	Gravity vector
T_m	External torque
E	Energy consumed by a flapping wing aircraft during a single flapping period
η	Energy conversion factor of the hollow cup motor
μ	Transmission angle
r	Penalty factor
ω_1, ω_2	Weighting factors

References

1. Chen, Y.; Zhao, H.; Mao, J.; Chirarattananon, P.; Helbling, E.F.; Hyun, N.P.; Clarke, D.R.; Wood, R.J. Controlled flight of a microrobot powered by soft artificial muscles. *Nature* **2019**, *575*, 324–329. [CrossRef]
2. Floreano, D.; Wood, R.J. Science, technology and the future of small autonomous drones. *Nature* **2015**, *521*, 460–466. [CrossRef] [PubMed]
3. Dong, X.; Xu, J.; Xu, X.; Dai, S.; Zhou, X.; Ma, C.; Cheng, G.; Yuan, N.; Ding, J. Sunlight-Driven Continuous Flapping-Wing Motion. *ACS Appl. Mater. Interfaces* **2020**, *12*, 6460–6470. [CrossRef] [PubMed]
4. Keennon, M.; Klingebiel, K.; Won, H. Development of the Nano Hummingbird: A Tailless Flapping Wing Micro Air Vehicle. In Proceedings of the 50th AIAA Aerospace Sciences Meeting Including the New Horizons Forum and Aerospace Exposition, Nashville, TN, USA, 9–12 January 2012.
5. Roshanbin, A.; Altartouri, H.; Karasek, M.; Preumont, A. COLIBRI: A hovering flapping twin-wing robot. *Int. J. Micro Air Veh.* **2017**, *9*, 270–282. [CrossRef]
6. Sun, J. Miniaturization of robots that fly on beetles' wings. *Science* **2020**, *370*, 1165. [CrossRef]
7. Lau, G.K.; Lim, H.T.; Teo, J.Y.; Chin, Y.W. Lightweight mechanical amplifiers for rolled dielectric elastomer actuators and their integration with bio-inspired wing flappers. *Smart Mater. Struct.* **2014**, *23*, 025021. [CrossRef]
8. Zhao, J.; Niu, J.; McCoul, D.; Leng, J.; Pei, Q. A rotary joint for a flapping wing actuated by dielectric elastomers: Design and experiment. *Meccanica* **2015**, *50*, 2815–2824. [CrossRef]
9. Phan, H.V.; Aurecianus, S.; Au, T.K.L.; Kang, T.; Park, H.C. Towards the Long-Endurance Flight of an Insect-Inspired, Tailless, Two-Winged, Flapping-Wing Flying Robot. *IEEE Robot. Autom. Lett.* **2020**, *5*, 5059–5066. [CrossRef]
10. Roshanbin, A.; Abad, F.; Preumont, A. Kinematic and Aerodynamic Enhancement of a Robotic Hummingbird. *AIAA J.* **2019**, *57*, 4599–4607. [CrossRef]
11. Coleman, D.; Benedict, M.; Hrishikeshavan, V.; Chopra, I. Design, development and flight-testing of a robotic hummingbird. In Proceedings of the AHS 71st Annual Forum, Virginia Beach, VA, USA, 5–7 May 2015; pp. 5–7.
12. Mishra, S.; Tripathi, B.; Garg, S.; Kumar, A.; Kumar, P. Design and Development of a Bio-Inspired Flapping Wing Type Micro Air Vehicle. *Procedia Mater. Sci.* **2015**, *10*, 519–526. [CrossRef]
13. Zhang, Y.; Wang, Z.; Zheng, H. Aerodynamic Analysis and Design Optimization of a Novel Flapping Wing Micro Air Vehicle in Hovering Flight. *J. Appl. Fluid Mech.* **2023**, *16*, 505–517. [CrossRef]
14. Isakhani, H.; Priestley, T.; Davis, S.; Nefti-Meziani, S. Design and Development of a Novel Insect-Inspired Flapping Mechanism. In Proceedings of the AIAA SCITECH 2025 Forum, Orlando, FL, USA, 6–10 January 2025.
15. Balachandar, N.; M, Y.; M, A.; Kesavan, M.; Unni, V.R. Actuator System for Directional Manoeuvre of a Flapping Wing Aerial Vehicle. In Proceedings of the AIAA SCITECH 2025 Forum, Orlando, FL, USA, 6–10 January 2025.
16. Conn, A.T.; Burgess, S.C.; Ling, C.S. Design of a parallel crank-rocker flapping mechanism for insect-inspired micro air vehicles. *Proc. Inst. Mech. Eng. Part C J. Mech. Eng. Sci.* **2007**, *221*, 1211–1222. [CrossRef]
17. de Croon, G.C.; Groen, M.A.; De Wagter, C.; Remes, B.; Ruijsink, R.; van Oudheusden, B.W. Design, aerodynamics and autonomy of the DelFly. *Bioinspir. Biomim.* **2012**, *7*, 025003. [CrossRef] [PubMed]

18. Gerdes, J.W.; Gupta, S.K.; Wilkerson, S.A. A Review of Bird-Inspired Flapping Wing Miniature Air Vehicle Designs. In Proceedings of the ASME International Design Engineering Technical Conferences/Computers and Information in Engineering Conference, Montreal, QC, Canada, 15–18 August 2010; pp. 57–67.
19. Hu, K.; Deng, H.; Xiao, S.; Yang, G.; Sun, Y. Design of a Bio-inspired, Two-winged, Flapping-wing Micro Air Vehicle with High-lift Performance. *J. Bionic Eng.* **2024**, *21*, 1191–1207. [CrossRef]
20. Rayman, B.; Jawad, B.; Vejdani, H. Design and Integration of a Flapping Wing Apparatus. *ASME Open J. Eng.* **2024**, *3*. [CrossRef]
21. Johansson, L.C. Aerodynamic efficiency explains flapping strategies used by birds. *Proc. Natl. Acad. Sci. USA* **2024**, *121*, e2410048121. [CrossRef]
22. Dickinson, M.H.; Lighton, J.R.B. Muscle efficiency and elastic storage in the flight motor of Drosophila. *Science* **1995**, *268*, 87–90. [CrossRef]
23. Sun, M.; Du, G. Lift and power requirements of hovering insect flight. *Acta Mech. Sin.* **2003**, *19*, 458–469.
24. Wang, Z.; Hu, X.; Wu, Y. Energy-efficient wing design for flapping wing micro aerial vehicles. *J. Mech. Sci. Technol.* **2019**, *33*, 4093–4104. [CrossRef]
25. Terze, Z.; Pandza, V.; Kasalo, M.; Zlatar, D. Optimized flapping wing dynamics via DMOC approach. *Nonlinear Dyn.* **2021**, *103*, 399–417. [CrossRef]
26. Tuncer, I.H.; Kaya, M. Optimization of flapping airfoils for maximum thrust and propulsive efficiency. *AIAA J.* **2005**, *43*, 2329–2336. [CrossRef]
27. Li, Q.; Ji, A.; Shen, H.; Li, R.; Liu, K.; Zheng, X.; Shen, L.; Han, Q. Experimental Study on the Wing Parameter Optimization of Flapping-Wing Aircraft Based on the Clap-and-Fling Mechanism. *Int. J. Aeronaut. Space Sci.* **2022**, *23*, 265–276. [CrossRef]
28. Ramezani, A.; Chung, S.J.; Hutchinson, S. A biomimetic robotic platform to study flight specializations of bats. *Sci. Robot.* **2017**, *2*, eaal2505. [CrossRef]
29. Karasek, M.; Muijres, F.T.; De Wagter, C.; Remes, B.D.W.; de Croon, G. A tailless aerial robotic flapper reveals that flies use torque coupling in rapid banked turns. *Science* **2018**, *361*, 1089–1094. [CrossRef]
30. Dickinson, M.H.; Lehmann, F.O.; Sane, S.P. Wing rotation and the aerodynamic basis of insect flight. *Science* **1999**, *284*, 1954–1960. [CrossRef] [PubMed]
31. Truong, Q.T.; Nguyen, Q.V.; Truong, V.T.; Park, H.C.; Byun, D.Y.; Goo, N.S. A modified blade element theory for estimation of forces generated by a beetle-mimicking flapping wing system. *Bioinspir. Biomim.* **2011**, *6*, 036008. [CrossRef] [PubMed]
32. Balli, S.S.; Chand, S. Transmission angle in mechanisms (Triangle in mech). *Mech. Mach. Theory* **2002**, *37*, 175–195. [CrossRef]
33. Myszka, D.H.; Murray, A.P.; Wampler, C.W. Computing the Branches, Singularity Trace, and Critical Points of Single Degree-of-Freedom, Closed-Loop Linkages. *J. Mech. Robot.* **2014**, *6*, 011006. [CrossRef]
34. Chen, J.; Yao, K.; Yu, C.; Xu, Y.; Zhou, S.; Ye, J. Synthesis of a single-degree-of-freedom noncircular pulley-five-bar finger rehabilitation mechanism considering force transfer performance. *Proc. Inst. Mech. Eng. Part C J. Mech. Eng. Sci.* **2025**, *239*, 55–70. [CrossRef]
35. Liu, X.W.; Dai, Y.H.; Huang, Y.K.; Sun, J. A Novel Augmented Lagrangian Method of Multipliers for Optimization with General Inequality Constraints. *Math. Comput.* **2023**, *92*, 1301–1330. [CrossRef]
36. Bai, J.; Jia, L.; Peng, Z. A New Insight on Augmented Lagrangian Method with Applications in Machine Learning. *J. Sci. Comput.* **2024**, *99*, 53. [CrossRef]
37. Alhijawi, B.; Awajan, A. Genetic algorithms: Theory, genetic operators, solutions, and applications. *Evol. Intell.* **2024**, *17*, 1245–1256. [CrossRef]

Disclaimer/Publisher's Note: The statements, opinions and data contained in all publications are solely those of the individual author(s) and contributor(s) and not of MDPI and/or the editor(s). MDPI and/or the editor(s) disclaim responsibility for any injury to people or property resulting from any ideas, methods, instructions or products referred to in the content.